Preprint/Prétirage

# Adaptive Compensation of RADARSAT SAR Analogue-to-Digital Converter Saturation Power Loss

P.W. Vachon, A.L. Gray, and C.E. Livingstone
Canada Centre for Remote Sensing
588 Booth St., Ottawa, Ont. K1A 0Y7 Canada
Phone: 613 995-1575 Fax: 613 947-1385
E-mail: paris.vachon@ccrs.nrcan.gc.ca

A.P. Luscombe
SPAR Aerospace
21025 Trans-Canada Highway,
Ste-Anne-de-Bellevue, Que. H9X 3R2 Canada
Phone: 514 457-2150 (x3641) Fax: 514 425-3041
E-mail: aluscomb@spar.ca

**Abstract**

Dark rangeward bands sometimes appear in RADARSAT synthetic aperture radar (SAR) imagery of the coastal zone. These bands may be visible over land or ice when water is in the near range. This artifact arises since RADARSAT's automatic gain control (AGC) is set by the near-half swath alone, while the far-half swath could return more power than the near-half swath, depending on scene content. If the gain is inappropriately set too high for the far-half swath, then the radar's 4-bit analogue-to-digital converter (ADC) will saturate, one effect of which is a loss in power and the appearance of the image banding. We have tested a simple correction methodology to improve image radiometry under these circumstances. Based upon measurement of the signal data variance and the power loss properties of a 4-bit ADC, an adaptive gain parameter is estimated which is used to scale the signal data and recover the lost power. As the ADC saturation represents a real information loss, the dynamic range of the rescaled image is reduced in the saturated regions. The methodology has been implemented for our workstation-based SAR processor. We describe the correction methodology and present some algorithm test results.

## 1 Introduction

An analogue-to-digital converter (ADC) will saturate if the input signal level exceeds the converter's dynamic range. When saturation occurs, the fidelity of the digitized signal is compromised, and non-linear effects such as power loss, small signal suppression, and degradation in the signal-to-noise ratio will occur.

For spaceborne synthetic aperture radar (SAR), the signal data are usually digitised on board the satellite and the digital numbers are downlinked to a ground station for compression and SAR image formation. SAR signal data are well-approximated as a Gaussian random variable. If the input signal exceeds the optimum input level of the ADC, a significant fraction of the digitized signal will be clipped, leading to power loss in the signal data and the resulting image. If the power loss is not compensated, the image radiometry will be inaccurate and calibration errors will occur.

Extensive work has been carried out to characterize and correct for saturation power loss of the ERS-1 SAR's 5-bit ADCs [Meadows and Wright, 1994] [Cooper, 1994]. In this case, the input signal data saturate for bright, distributed targets, such as the ocean surface under high wind speed conditions. Compensation for ADC power loss is essential if accurate calibration is required for ocean or coastal scenes. The problem has been ameliorated for ERS-2 by a reduction of the on board gain prior to the ADC.

For the RADARSAT SAR, the problem is more subtle. RADARSAT's automatic gain control (AGC) is intended to adjust the signal data level for optimum use of the radar's 4-bit ADC dynamic range. Unfortunately, due to an implementation decision, the AGC is controlled by samples 1025 to 3072 of the signal data which cover only a portion of the scene in the near-half swath. If lower return power occurs in the near-half swath than in the far-half swath, then the gain could be too high in the far-half swath, resulting in ADC saturation and power loss. For a C-band HH polarization radar such as RADARSAT, water surfaces generally have lower cross section than land, especially for larger incidence angles. The power loss can manifest itself in SAR images as a rangeward-oriented dark band of power loss in the event of spatially varying return power in the near-half swath. Associated with the power loss is a reduction in scene dynamic range caused by the clipping of all stronger returns to the maximum ADC level. Saturation can occur over land in the far-half swath for coastal regions with islands and embayments in the near-half swath. On the other hand, if the near-half swath is of uniformly low returned power, as could occur for coastal regions with more linear shorelines, then broader expanses of power loss could also occur over land in the far-half swath, similar to the problem which exists over the ocean for ERS-1. In this case, power loss could be present, but without noticeable rangeward banding.

In this paper, we consider a compensation for lost power in RADARSAT SAR images [Vachon *et al.*, 1996] [Vachon, 1997]. The technique is closely related to procedures used for the ERS SARs, in which analysis of signal data variance over a ground footprint allows estimation of the lost power and the derivation of a gain correction which may be applied to the signal data or to the image. The complication with RADARSAT is that the AGC leads to varying gain in azimuth. Therefore, the correction is best-applied to the signal data prior to compression. A disadvantage with RADARSAT is that many different gains could occur over a single ground footprint. Therefore, more localized signal data statistics must be considered in estimating the gain correction. There are various ways of choosing the applied gain, depending on the compensation criteria [Cooper, 1994] [Husøy and Bugge, 1997].

In Section 2, we outline the adaptive algorithm used to correct RADARSAT SAR data for ADC saturation power loss. In Section 3, we present two examples which serve to illustrate the performance of the algorithm. In Section 4, we discuss some other possible effects of ADC saturation.

# 2 Algorithm

Two examples of signal data histograms for a 4-bit ADC subject to a Gaussian noise input are shown in Fig. 1. As the input variance increases, the degree of saturation also increases. As saturation occurs, the output variance increases but less rapidly, as illustrated in Fig. 2 which shows the relationship between the ratio of the input and output signal variance for a 4-bit ADC with various Gaussian noise inputs. This curve represents the ADC power loss characteristic for a distributed scene. Note that signal underflow occurs for low input variance. Although we have considered only the observed signal data variance, there are other possible characterizations of the degree of saturation. For example, the saturation count (joint or single channel) could be used. However, use of the variance also allows estimation and limited compensation for signal data underflow.

The generic power loss correction scenario proceeds as follows. The I-channel signal data variance is measured. The corresponding power loss is looked-up using the appropriate power loss characteristic (Fig. 2 for RADARSAT or the corresponding 5-bit curve for ERS). The signal data are then scaled to compensate for the lost power.

This procedure is well-known for the ERS-1 SAR [Meadows and Wright, 1994] [Scoon *et al.*, 1996]. An example of power loss compensation for an ERS-1 SAR ocean image is shown in Fig. 3. In this case, the radar cross section profile as a function of incidence angle is compared with a model prediction driven by an *in situ* wind vector measurement, both with and without ADC power loss correction [Vachon and Dobson, 1996]. Following correction, there is excellent agreement between the model prediction and the observed profile in terms of the absolute radar cross section level and slope. ADC saturation power loss compensation is essential for ERS-1 SAR images over the ocean.

For the RADARSAT case, there are some additional complications. Ideally, we would like to estimate the power loss over each ground footprint. However, due to the operation of the AGC, the gain could change as frequently as every 8th range line. Our implementation involves estimating the I-channel signal data

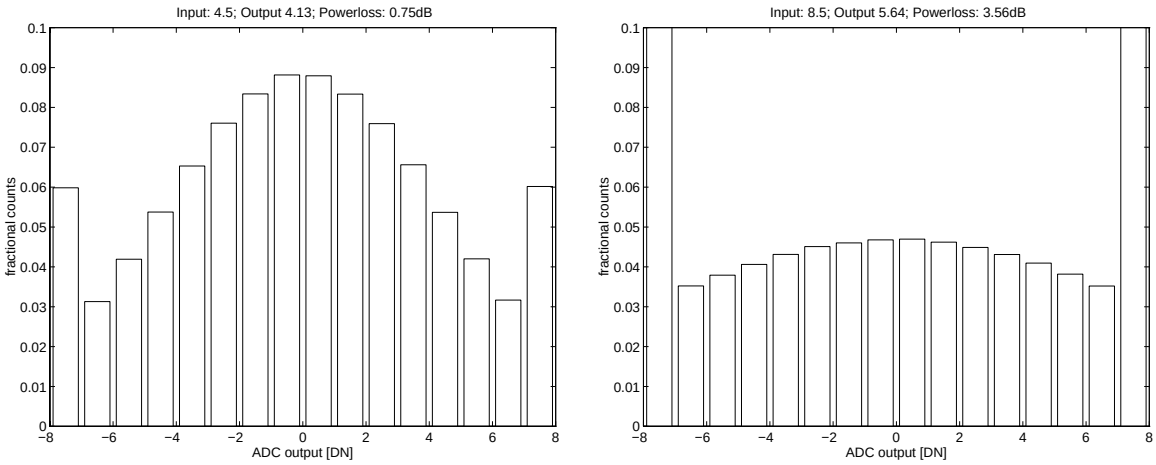


Figure 1: *Behaviour of a 4-bit ADC subject to a Gaussian noise input.*

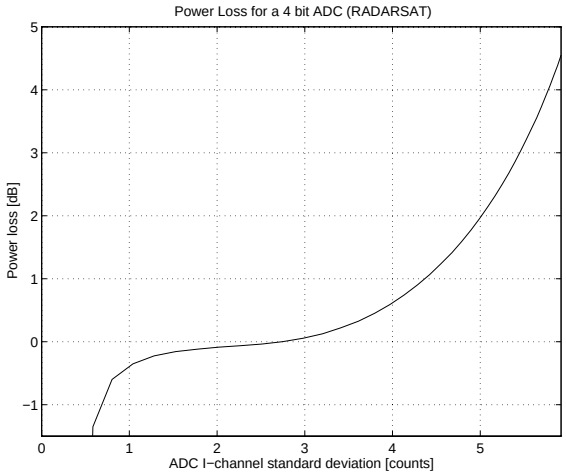


Figure 2: *4-bit ADC power loss characteristic*

variance over azimuth blocks having constant gain, and over range blocks of fixed size. We then apply a median filter in range to retrieve a smoothed variance estimate. The power loss is estimated for the centre of each block and is calculated for each signal data point by using linear interpolation between the block centres.

We have tested this algorithm at CCRS using dtSAR, a flexible workstation-based implementation of the RADARSAT Canadian Data Processing Facility (CDPF) SAR processor. Our initial implementation was completed in August 1996 and was based on a modification of the 4-bit signal data file on disk [Vachon *et al.*, 1996]. The statistics were collected as described above, the data were scaled, then re-mapped back to 4-bits with a new gain setting chosen to preserve the dynamic range of the scaled data. This algorithm presented the possibility of underflow for low signal regions, but was low risk since modification of the processor was not required. Following encouraging testing, a more robust implementation was carried out as part of the processor's ingest operation in December 1996. Now, a set of scalar gains are calculated as the signal data are read from tape to disk. The gains are then applied after the data are converted to floating point in the processor. This implementation is more accurate than the 4-bit to 4-bit remapping and avoids problems with data underflow.

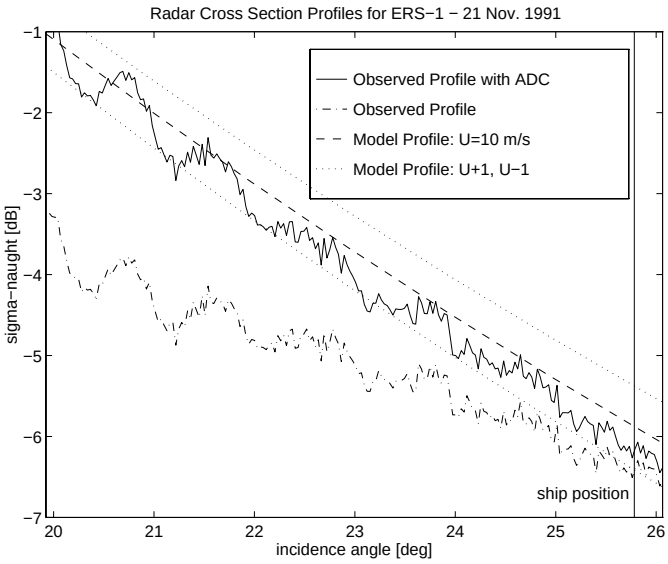


Figure 3: *Example of ADC power loss correction for ERS-1 SAR*

# 3 Example Results

## 3.1 Juan de Fuca Strait

Fig. 4 shows an example RADARSAT image of Juan de Fuca Strait with an extreme ADC power loss artifact. The artifact arose when the darker water occupied all of the near-half swath, thus driving the gain up, and causing ADC saturation and power loss in the far-half swath. The upper panel shows the original image, while the lower panel shows the image following the power loss correction described above. Note that the visual impact of the power loss artifact is significantly reduced. Before and after correction relative radar cross section transects through the artifact are shown in Fig. 5. The azimuth transect was taken near the far right and spans an azimuth extent beyond that included in Fig. 4. The range transect was taken down the middle of the artifact. The maximum power loss in this case was around 7 dB. However, the residual artifact after compensation appears to be $< 1$ dB.

## 3.2 Lake Winnipeg

Fig. 6 shows a pair of RADARSAT SAR images acquired over the north-east shore of Lake Winnipeg. The images were acquired using the same beam mode, were taken from ascending and descending passes, and were separated in acquisition time by roughly 12 hours. Due to the short time interval between passes, we can assume that the land signature is the same in both cases. This image pair was acquired so that land occupied the near-half of the descending pass (hence correct gain setting for the land) and water occupied the near-half of the ascending pass (hence correct gain setting for water, but high gain and power loss over land in the far-half). Rangeward transects of relative radar cross section are shown in Fig. 7. Although both images look radiometrically smooth, it is apparent from the transects that, assuming that the relative cross section profile over land should be contiguous with incidence angle, there is a $\sim 2$ dB power loss for the ascending pass. Following power loss correction, the transect over land is essentially contiguous between the descending pass and the power loss corrected ascending pass, indicating that the correction is reasonably accurate in this case, for which the degree of power loss was not too large.

# 4 Other Saturation Effects

Saturation power loss is only one possible effect of ADC saturation and is the only effect which is compensated by the procedure outlined above. For example, signal data saturation could also lead to small signal

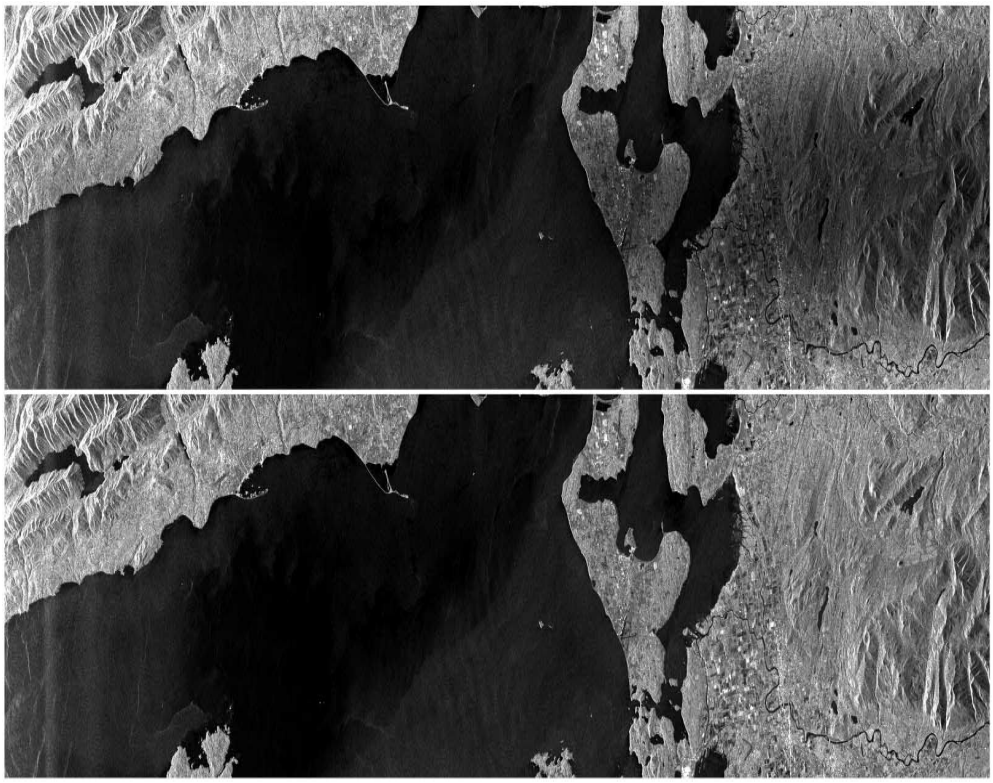

Figure 4: *Example RADARSAT SAR W2 image of Juan de Fuca Strait having an ADC power loss artifact before (top) and after (bottom) correction acquired 14 Jan. 1996. Azimuth is bottom-to-top while ground range is left-to-right. Each image covers 33 km in azimuth by 160 km in ground range.* ©*CSA 1996.*

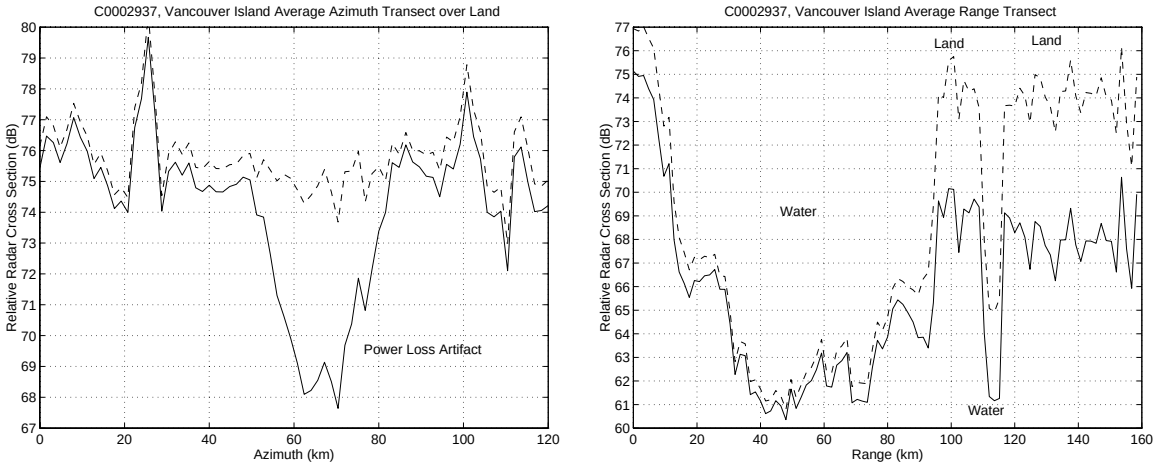


Figure 5: *Relative radar cross section transects for the Juan de Fuca Strait image.*

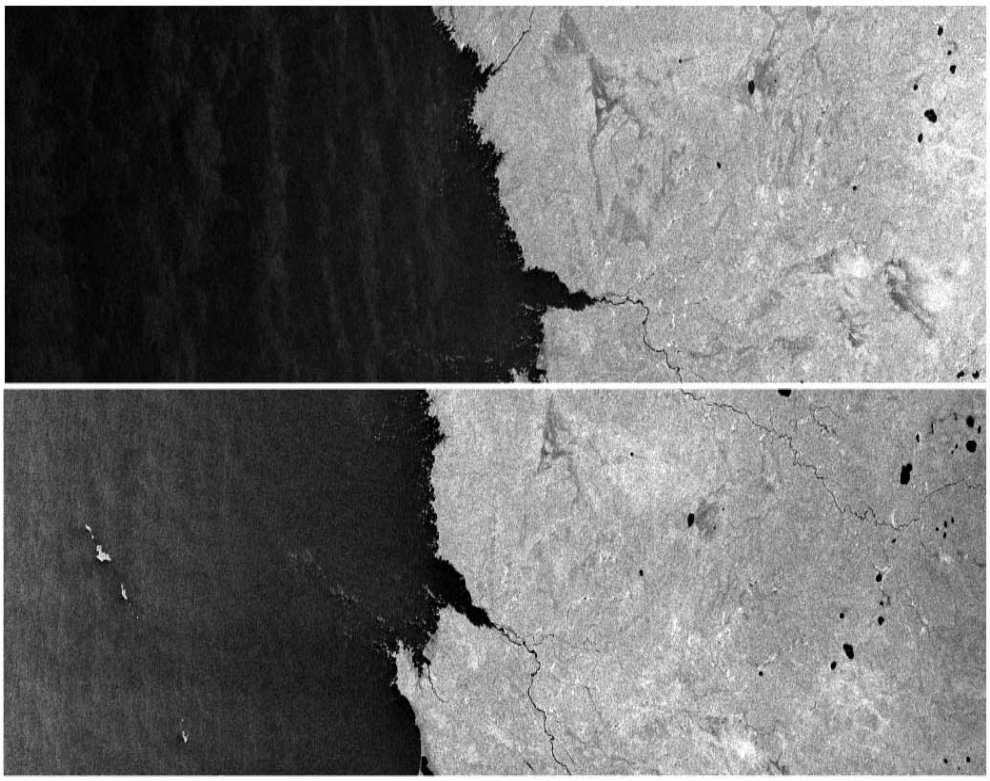

Figure 6: *RADARSAT SAR S3 images of the north-east shore of Lake Winnipeg acquired 17 Oct. 1996 12:48 descending (top) and 18 Oct. 1996 00:13 ascending (bottom). For the top image, azimuth is top-to-bottom while ground range is right-to-left. For the bottom image, azimuth is bottom-to-top while ground range is left-to-right. Each image covers 28 km in azimuth by 112 km in ground range. The images are skewed with respect to one another.* ©*CSA 1996.*

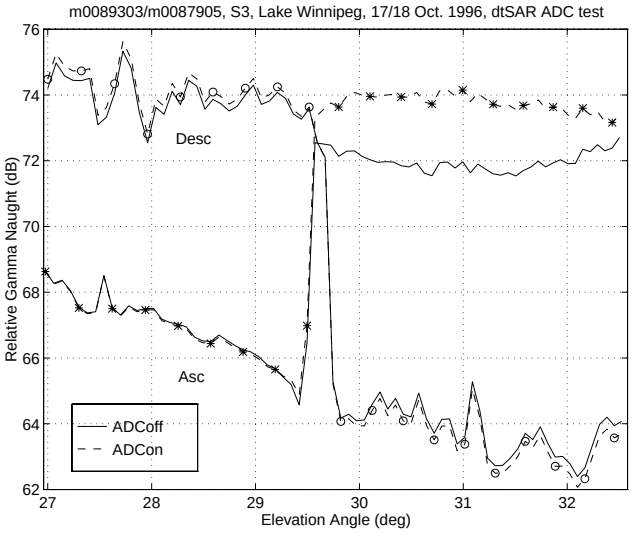


Figure 7: *Relative radar cross section transects for the Lake Winnipeg images.*

Table 1: *Possible RADARSAT SAR ADC power loss scenarios.*

| near | far | |
|---|---|---|
| water | land | water OK, possible land saturation and SSS near coast |
| land | water | land OK, possible underflow for water |

Table 2: *Results of 5-bit Gaussian noise processing test.*

| std. in [counts] | std. out [counts] | sat. [%] | Ploss [dB] | MSVR | skewness | kurtosis |
|---|---|---|---|---|---|---|
| 5 | 5.00 | 0.3 | 0.0 | 3.00 | 1.158 | 5.025 |
| 10 | 8.95 | 13.4 | -1.0 | 3.00 | 1.158 | 5.030 |
| 15 | 11.01 | 31.8 | -2.7 | 3.00 | 1.152 | 4.978 |
| 20 | 12.13 | 45.4 | -4.3 | 3.01 | 1.151 | 4.987 |
| 25 | 12.81 | 55.0 | -5.8 | 2.99 | 1.165 | 5.065 |
| Gaussian | | | | 3.00 | 1.155 | 5.000 |

suppression (SSS), in which small signals are obliterated if they occupy the same footprint as a saturated region [Livingstone *et al.*, 1983]. The scope of this effect may be judged from the ground extent of the range chirp (6.3 km in slant range) and the azimuth beamwidth (roughly 4 km). Saturation could also degrade the signal-to-noise ratio and could locally change the image texture, which could be significant for certain SAR classification schemes. The occurrence and extent of ADC saturation is summarized in Table 1. To illustrate how ADC saturation can change image texture, we consider two SAR processing tests.

## 4.1 Gaussian Noise Test

Both SAR processing tests were carried out for the 5-bit ERS case. In the first test, we generated circular Gaussian noise files with various standard deviations, converted the noise files to 5-bits with saturation, and processed the noise to the ERS precision image ($L = 3$ independent looks) standard. We then measured the image statistics to determine the departures, if any, from $\chi^2_{2L}$ for which we expect the first three normalized moments to be: mean-squared-to-variance ratio, MSVR $= L$; skewness $= \sqrt{4/L}$; and kurtosis $= 3 + 6/L$. The results are presented in Table 2. Perhaps surprisingly, the image statistics are essentially $\chi^2_{2L}$ for all cases considered, independent of the degree of signal data saturation. This result serves to demonstrate the power of the central limit theorem applied to the large number of samples in the footprint of a polar orbiting C-band SAR. However, the occurrence of extensive Gaussian-distributed scenes is rather rare.

## 4.2 ERS-1 Signal Data Overflow Test

To better understand the effects of ADC saturation on a SAR scene with real texture, in the second SAR processing test we selected an ERS-1 SAR signal data set which we bit shifted to produce 1-, 2-, 3-, 4-, and 5-bit signal data sets with varying degrees of saturation. The data were processed to the precision image standard (in this case $L = 2.9$ independent looks due to the weighting of the ERS-1 antenna pattern). The resulting SAR images are shown in Fig. 8. Note that each image looks satisfactory radiometrically in spite of some having high levels of signal data saturation. The statistics from a homogeneous image region were extracted and checked for divergence from $\chi^2_{2L}$ and for any saturation dependence. The results are presented in Table 3. Note that the statistics are not Gaussian and depend upon the number of bits (and degree of saturation) to which the signal data were processed. The increasing MSVR and decreasing skewness and kurtosis with increasing signal data saturation serve to illustrate the reduction in image dynamic range associated with signal data saturation.

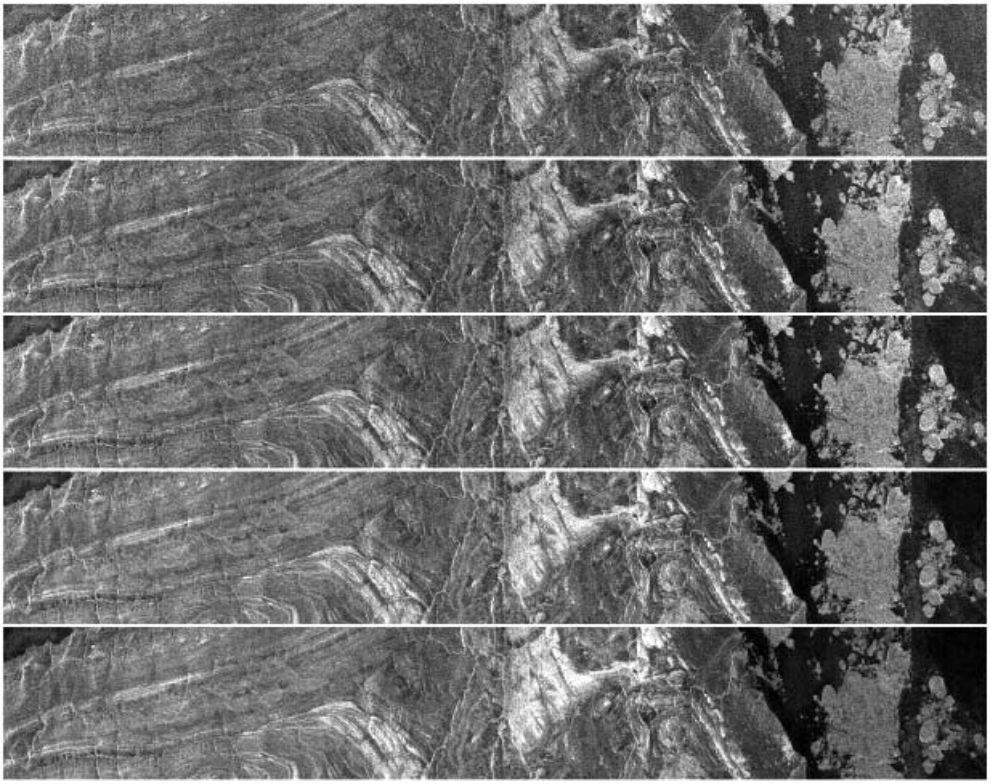

Figure 8: *ERS-1 SAR image of Bathurst Island acquired 10 Feb. 1992. The signal data were processed with 1-bit (top) through 5-bit (bottom). Azimuth is from top-to-bottom while ground range is from right-to-left. Each image covers 11 km in azimuth by 39 km in ground range. ©ESA 1992.*

Table 3: *Results of ERS-1 bit shifting test.*

| bits | std. out [counts] | sat. [%] | Ploss [dB] | MSVR | skewness | kurtosis |
|---|---|---|---|---|---|---|
| 1 | 0.50 | 100.0 | -22.5 | 2.58 | 1.45 | 6.69 |
| 2 | 1.41 | 87.2 | -13.4 | 2.50 | 1.51 | 7.26 |
| 3 | 2.95 | 62.2 | -6.8 | 2.42 | 1.58 | 7.91 |
| 4 | 4.92 | 24.8 | -2.1 | 2.33 | 1.64 | 8.46 |
| 5 | 6.00 | 1.3 | -0.1 | 2.29 | 1.66 | 8.44 |
| Gaussian | | | | 2.90 | 1.17 | 5.07 |

# 5 Conclusions

We have demonstrated an algorithm which quantitatively corrects power loss associated with ADC saturation, a known problem with RADARSAT SAR image radiometry which is caused by inappropriate gain setting by the AGC. The algorithm is data adaptive and can correct for localized rangeward artifacts as well as broader expanses of power loss which may not have a visible image signature. Scalar gain corrections are derived from the signal data variance calculated on a block-by-block basis and the 4-bit ADC power loss characteristic. The algorithm assumes a Gaussian distributed signal data input and that the non-linearity is restricted to the ADC.

The Juan de Fuca Strait example illustrated that the algorithm is able to reduce a rangeward power loss artifact $\sim 7$ dB to a residual of $< 1$ dB. Visually, the image was significantly improved. The Lake Winnipeg

example illustrated that power loss could exist in RADARSAT SAR images even if it is not visually apparent by inspection of the image. Furthermore, this example illustrated that if the power loss is $< 3$ dB, say, then the algorithm does a good job of recovering the lost image power.

An alternate strategy to eliminate power loss artifacts is to use a constant (*i.e.* fixed) acquisition gain. This approach is currently in use and requires that the user specify the acquisition gain to be used. While this solves the radiometric banding problem from an image cosmetics point of view, it is difficult to specify this gain setting for an arbitrary target, especially for the ocean which presents a large range of radar cross sections as a function of sea state and wind speed. Therefore, ADC saturation and power loss could still occur. Even with fixed gain, the proposed algorithm would allow any ADC saturation power loss to be corrected.

Although radiometric calibration should be treated with extreme caution whenever ADC saturation occurs, it is evident that the reported algorithm significantly reduces the visual impact of power loss artifacts. As such, it is recommended that this procedure be incorporated in the CDPF. This would allow improved radiometry for both archived data acquired with AGC enabled and data acquired with fixed gain.

The algorithm does not address possible corruption of image texture, small signal suppression in the coastal zone, or degraded signal-to-noise ratio caused by ADC saturation. Two processing experiments indicate that input Gaussian noise always leads to a $\chi^2_{2L}$ distributed image, independent of the degree of saturation, but that image texture and dynamic range is dependent on the degree of signal data saturation for non-Gaussian scenes. Therefore, we expect that image texture could be compromised if significant signal data saturation has occurred.

# 6 Acknowledgements

We thank J. Campbell (Intermap), R. Hawkins (CCRS), P. Lim (MDA), T. Lukowski (CCRS), R. Touzi (CCRS), L. Wilke (MDA), and J. Wolfe (Intermap) for their contributions to this work, which was carried out in the context of RADARSAT ADRO Project #160. The Lake Winnipeg images were obtained through RVP. The implementation of the power loss correction procedure as an integral part of dtSAR was carried out by MDA under contract to CCRS.

# References

Cooper, P. S., ADC saturation effects and point target calibration, in *Proc. CEOS SAR Calibration Workshop, 28–30 September 1994, Ann Arbor, Michigan, USA*, pp. 38–50, 1994.

Husøy, P. O., and H. Bugge, Correction of saturation artifacts in SAR images, in *Proc. of a Workshop on RADARSAT Data Quality, 4–6 February 1997, St-Hubert, Quebec, Canada*, CEOS Working Group on Calibration and Validation, SAR Calibration Subgroup, Appendex E.5, RADARSAT Processing, 1997.

Livingstone, C. E., D. Hudson, J. D. Lyden, C. Liskow, R. Shuchman, and R. Lowry, Gain compression effects in SAR imagery, in *Proc 17th International Symposium on Remote Sensing of the Environment, 9-13 May 1983, Ann Arbour, U.S.A.*, pp. 1109–1116, 1983.

Meadows, P. J., and P. A. Wright, ERS-1 SAR Analogue to Digital Converter Saturation, in *Proc. CEOS SAR Calibration Workshop, 28–30 September 1994, Ann Arbor, Michigan, USA*, pp. 24–37, 1994.

Scoon, A., I. S. Robinson, and P. J. Meadows, Demonstration of an improved calibration scheme for ERS-1 SAR imagery using a scatterometer wind model, *Int. J. Rem. Sens.*, *17*(2), 413–418, 1996.

Vachon, P. W., A correction for RADARSAT SAR ADC saturation, in *Proc. of a Workshop on RADARSAT Data Quality, 4–6 February 1997, St-Hubert, Quebec, Canada*, CEOS Working Group on Calibration and Validation, SAR Calibration Subgroup, Appendex E.3, Radiometric Calibration, 1997.

Vachon, P. W., and F. W. Dobson, Validation of wind vector retrieval from ERS-1 SAR images over the ocean, *The Global Atm. and Ocean Syst.*, *5*, 177–187, 1996.

Vachon, P. W., A. L. Gray, and A. P. Luscombe, RADARSAT SAR analogue-to-digital converter saturation, in *Proc. The 6th Workshop of the Canadian Ice Working Group, RADARSAT for Ice and Oceans, Early Experience and Data Access, 19–21 November 1996, Ottawa, Canada*, Joint Session - 10 minute presentation, 1996.